This article has been accepted for inclusion in a future issue of this journal. Content is final as presented, with the exception of pagination.

Self-Powered Wireless Affinity-Based Biosensor Based on Integration of Paper-Based Microfluidics and Self-Assembled RFID Antennas

Mingquan Yuan, *Student Member, IEEE*, Evangelyn C. Alocilja, *Member, IEEE*, and Shantanu Chakrabartty, *Senior Member, IEEE*

***Abstract*—This paper presents a wireless, self-powered, affinity-based biosensor based on the integration of paper-based microfluidics with our previously reported method for self-assembling radio-frequency (RF) antennas. At the core of the proposed approach is a silver-enhancement technique that grows portions of a RF antenna in regions where target antigens hybridize with target specific affinity probes. The hybridization regions are defined by a network of nitrocellulose based microfluidic channels which implement a self-powered approach to sample the reagent and control its flow and mixing. The integration substrate for the biosensor has been constructed using polyethylene and the patterning of the antenna on the substrate has been achieved using a low-cost ink-jet printing technique. The substrate has been integrated with passive radio-frequency identification (RFID) tags to demonstrate that the resulting sensor-tag can be used for continuous monitoring in a food supply-chain where direct measurement of analytes is typically considered to be impractical. We validate the proof-of-concept operation of the proposed sensor-tag using IgG as a model analyte and using a 915 MHz Ultra-high-frequency (UHF) RFID tagging technology.**

***Index Terms*—Flexible electronics, ink-jet printing, micro-monopole antenna, paper-based microfluidics, radio-frequency identification (RFID), self-assemble, self-powered sensing, silver enhancement, wireless biosensor.**

I. Introduction

PAPER based microfluidics devices, also known as "lab on paper", is an active area of research because it provides a simple, low-cost platform to analyze liquid samples in the field. Examples of such platform include biological assays that can detect and measure different concentration levels of *Salmonella* [1], [2], glucose [3], [4], cholesterol [5] and protease [6]. The principle underlying all these paper-based platforms is to immobilize protein-based reactive elements (enzymes, antibodies, aptamers, peptides or DNA) on paper in conjunction with a transducer that converts the binding of the target analyte with the protein into a measurable signal. Broadly these devices can be categorized into four classes based on their detection method [7]: a) colorimetric detection [2]; b) electrochemical (EC) detection [3], [5]; c) chemiluminescence (CL) detection [4] and d) electrochemiluminescence (ECL) detection [8]. Colorimetric method is useful when a yes/no answer (target present or absent) is sufficient, whereas the EC method is used when a high detection sensitivity is required. The CL and ECL methods have not been widely used for paper-based biosensors since they require an optical-shield for read-out. Irrespective of their read-out methods, all these techniques require a direct access to the biosensor (optically or electrically), and hence cannot be used under scenarios when the samples to be analyzed are concealed. The scenario routinely occurs in food and medicinal supply-chain where the samples are packaged and shipped in sealed containers. For such applications there exists a need to monitor the quality of the product at every point of the supply-chain (without opening the package) so as to prevent and track the source of any contamination due to food-borne pathogens. However, monitoring at every point in the product supply-chain could be overwhelming due to the volume and rate of the products and the due to the detrimental effects of false-positives.

Fortunately, two converging economic trends have now made the vision of end-to-end supply-chain monitoring a reality. The first trend is that over the last decade the price of passive radio-frequency identification (RFID) tags have reduced by orders of magnitude when compared to the cost of packaging or materials [9], [10]. As a result, it is now economically viable to embed or attach a passive tag to every package of food-item. The second trend is that the new generation of smart-phones are equipped with the capability to read RFID tags. Given the rapid penetration of smart-phones in the consumer market, the tags can be interrogated at different segments of the supply-chain, as shown in Fig. 1, starting from the food-source all the way to the market shelves. Thus, and integrated platform combining the low-cost, paper-based microfluidic sensors with practically inexpensive passive RFID tags could be an attractive technology to continuously and wirelessly monitor the quality of a food-product in a supply-chain.

Unfortunately, most passive RFID based biosensors reported in the literature suffer from low reliability when detecting target analytes under real-world operating conditions. This is because

Manuscript received October 2, 2015; revised January 24, 2016; accepted February 22, 2016. This work was supported in part by the National Science Foundation under Research Grant CCF: 1117186 and in part by a Research Grant from the Research Institute for Value Chain Creation (MRIVCC). This paper was recommended by Associate Editor J. Blain.

M. Yuan and S. Chakrabartty are with the Department of Computer Science and Engineering, Washington University in St. Louis, St. Louis, MO 63130 USA (e-mail: mingquan@email.wustl.edu; shantanu@seas.wustl.edu).

E. C. Alocilja is with the Department of Biosystems and Agricultural Engineering, Michigan State University, East Lansing, MI 48824 USA (e-mail: alocilja@egr.msu.edu).

Color versions of one or more of the figures in this paper are available online at http://ieeexplore.ieee.org.

Digital Object Identifier 10.1109/TBCAS.2016.2535245

1932-4545 © 2016 IEEE. Personal use is permitted, but republication/redistribution requires IEEE permission.
See http://www.ieee.org/publications_standards/publications/rights/index.html for more information.

This article has been accepted for inclusion in a future issue of this journal. Content is final as presented, with the exception of pagination.

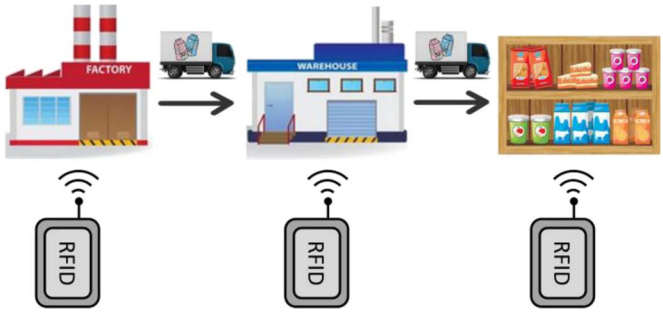

Fig. 1. Illustration of end-to-end monitoring of food quality in a supply-chain where RFID based biosensors can be interrogated at different locations of the supply-chain.

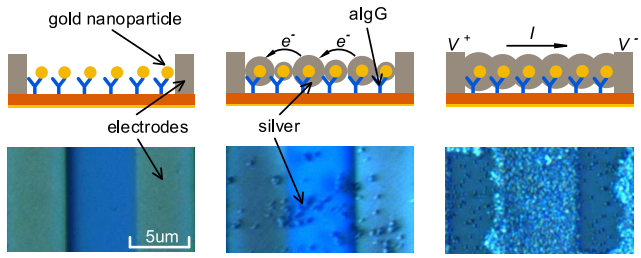

Fig. 2. Three stages of the silver-enhancement process. (a) Isolation mode: before the silver enhancement solution applied, the electrodes are electrically isolated. (b) Subthreshold mode: during the silver enhancement process, the silver ions get reduced to form metallic silver. (c) Above-threshold mode: more silver ions are reduced and the path between the two electrodes are electrically bridged [12].

these sensors detect binding of target analytes by measuring the deterioration in the tag's RF reflection properties which manifests itself as a shift in the antenna's center frequency or the reduction in the antenna's quality factor. Unfortunately, other environmental factors could also degrade and detune the tag antenna which produces false-positives. In [11]–[14] we had presented a novel approach of RFID biosensing based on the concept of "growing" RF antennas only when target analytes are present in the sample. This method of sensing can be viewed as a process that evolves from a disassembled detuned antenna to an assembled tuned antenna. While there can be numerous states of a disassembled antenna, there are only a few configurations that represent a assembled and tuned antenna. Therefore, it is highly unlikely that random environmental processes could produce a low-entropy state of a tuned antenna and hence the process of antenna self-assembly should produce lower false-positives compared to the traditional detuning approach. The challenge in designing the proposed self-assembly based sensor is to be able to control the process of antenna growth on the passive RFID tag, given that there are no continuously available power sources. Addressing some of these challenges is one of the goals of this paper.

First, we show that paper-based microfluidics can be used for low-cost and self-powered sample acquisition, sample flow and sample mixing. Second, we show that the microfluidic network can be integrated with a low-cost, ink-jet printed antennas on a plastic substrate. Third we demonstrate a proof-of-concept detection using an integrated commercial RFID tag compliant with the Gen-2 ultra-high-frequency (UHF) standard. This paper is organized as follows: Section II briefly introduces the principle of operation including silver enhancement technique and paper-based microfluidics followed by a describing a method to integrate the two approaches on an RFID platform. In Section III, we describe the materials and methods used to prepare our experimental setup. Section IV presents measurements obtained using the proposed biosensor and Section V concludes the paper with the discussions of the future work.

II. Principle of Operation

A. Self-Assembly of Antenna Elements

The basic principle of self-powered assembly and the growth of RF antenna elements is illustrated in Fig. 2. The figure shows two electrodes that are separated by a gap where gold nanoparticles (AuNPs) conjugated antibodies are immobilized. Because the dimensions of AuNPs are in a scale of nanometers, they are not large enough to electrically bridge the two separated electrodes. As a result, the two electrodes are in a open circuit state [Fig. 2(a)]. Once the silver enhancement solution (comprising of silver ions (Ag^{+}) and hydroquinone, a photographic developing solution) is applied in the gap, silver ions start reducing into metallic silver on the surface of the gold nanoparticles. This process is completely self-powered by the chemical activation energy and does not require any external biasing. Also, during this process, AuNPs serve as a catalyst and facilitate further reduction of silver-ions. As time progresses, more silver ions are reduced and a chain of AuNPs cored silver micro-monopole antennas assemble between the two electrodes, as shown in Fig. 2(b). Electrons can now hop between the two electrodes since the grown micro-monopole antennas provides shorter path compared with that shown in Fig. 2(a). Note that at this stage a complete micro-monopole antenna chain bridging the two electrodes has not yet formed. Given sufficient time and enough analytes, more silver ions get reduced and in the limit the two electrodes can be completely electrically bridged with the chain of micro-monopole antennas, as shown in Fig. 2(c). A relationship between the time of silver enhancement process and the size of self-assembled silver particles is shown in Fig. 3. When sufficient silver enhancement solution is present, the increase of the particle size is monotonic and almost linear with respect to the time of silver enhancement process. In [15] we reported that the conductance measured between the electrodes after the silver enhancement process is monotonic with respect to the concentration of the target analyte. The change in conductance could potentially change the reflectance property of the self-assembled RF antenna which can then be used to infer the concentration of the target analyte.

B. Integration With Paper-Based Microfluidics

One of the focus of this paper is to show that the principle of RF antenna self-assembly can be integrated with paper-based microfluidics by selecting the regions where silver-enhancement could occur. Most of the paper-based microfluidics devices are fabricated by patterning hydrophilic channels and hydrophobic

This article has been accepted for inclusion in a future issue of this journal. Content is final as presented, with the exception of pagination.

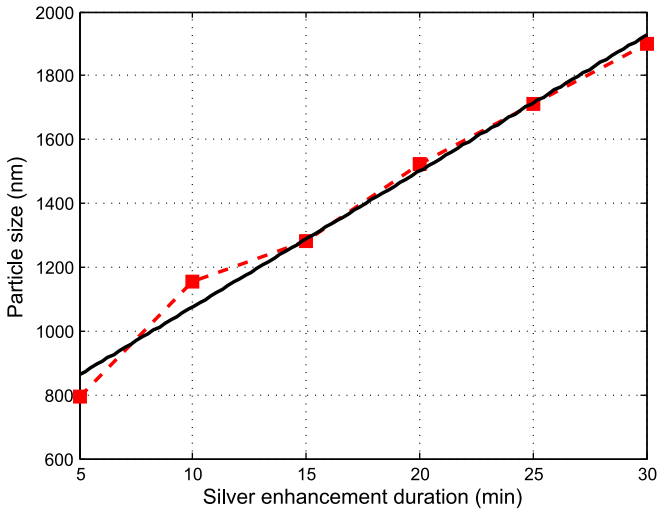

Fig. 3. Relationship showing the size of reduced silver particles and the total silver enhancement duration.

barriers on cellulose-based paper membranes, such as cellulose chromatography papers [16] and cellulose filter paper [17]. In this paper, we have used nitrocellulose membranes (manufactured by Millipore) as our microfluidics substrate due to its high antibody binding capacity and consistent pore size [18]. This is important because the length of the microfluidic channels is determined by the degree of penetration of the liquid through the porous nitrocellulose membrane, which is approximately modeled by the Washburn's equation [17] as

$$L = \sqrt{\frac{\gamma R \cos\theta}{2\eta} t} \tag{1}$$

where L is the liquid penetration distance in the paper, R is the average radius of pore size, γ is the surface tension of the liquid, η is the liquid viscosity and t is the time of the penetration. Both the parameters L and t have been used to optimize the size of the microfluidic channels as discussed in Section IV. Also for the sake of reliability, in this paper we have avoided the use of photolithography and wax printing to form reagent channels. Instead we have resorted to laser cutting to create different shapes that can function as liquid channels. Note that laser-ablation will typically burn the walls of the nitro-cellulose membrane. However, we only cut the 4 mil plastic backing on the nitrocellulose membrane (both HF13504XSS and HF18004XSS). We carefully adjusted the power/current and the cutting speed of the Full Spectrum Laser LLC MLE-40 to make sure the membrane is not over burned. After this laser pre-treatment, a razor blade is used to cut through the desired shape along the lines created by the laser cutting on the plastic substrate. The flow of the reagents through the channel is self-powered through capillary force of the membrane and the rate of the flow is controlled by changing the channel width. This can be used to control the rate of flow of the silver-enhancement solution as illustrated in Fig. 4. The region where silver enhancement occurs is the area (depicted by the labeled black box) where the two nitrocellulose membranes face each other. When the silver enhancement solution is applied to the application pad, it diffuses

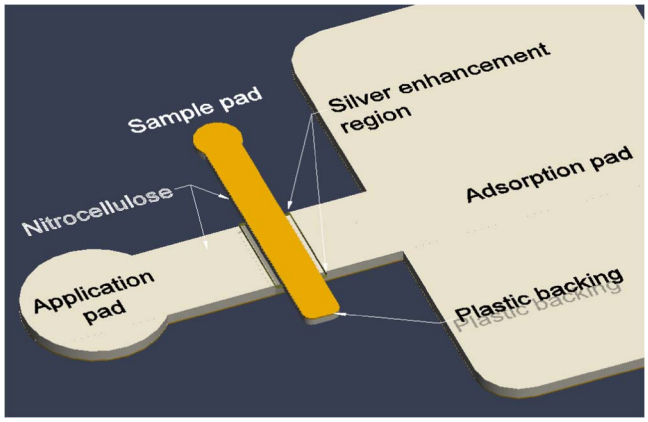

Fig. 4. Concept of integrating the principle of silver enhancement with paper-based microfluidics.

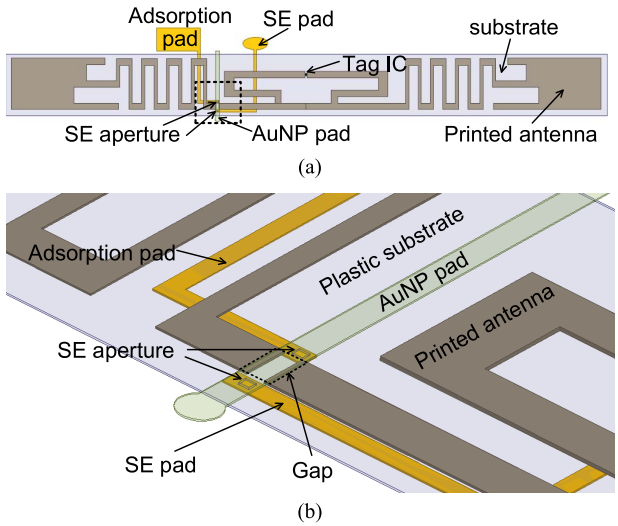

Fig. 5. Assembly and integration of microfluidics channels within the RFID biosensor. (a) Schematic of the self-powered microfluidics RFID biosensor. (b) Magnification of the area marked in Fig. 5(a).

through the nitrocellulose channel to the adsorption pad and in the process it interacts with the gold-nanoparticles located in the target area.

A visualization of a complete RFID antenna with an integrated microfluidic platform is shown in Fig. 5 where a dipole antenna structure is printed on the mesoporous substrate, as shown in Fig. 6. We will refer to the side of the substrate where the antenna is printed as the "front side" and the opposite side that does not contain printed antenna will be referred to as the "back side." Two small apertures are created on the polyethylene substrate on two sides of the gap, labeled as "SE aperture" in Fig. 5(b). These two SE apertures provide a path for the silver enhancement reagent to flow from the back side of the substrate. The antenna gap is covered with a nitrocellulose membrane ("AuNP Pad") with the nitrocellulose side facing the gap on the front side. The "SE Pad" and "Adsorption Pad" are then attached on the back side of the substrate with the nitrocellulose side facing the SE apertures, as shown in Fig. 5(b). These three pads serve as reservoirs which

This article has been accepted for inclusion in a future issue of this journal. Content is final as presented, with the exception of pagination.

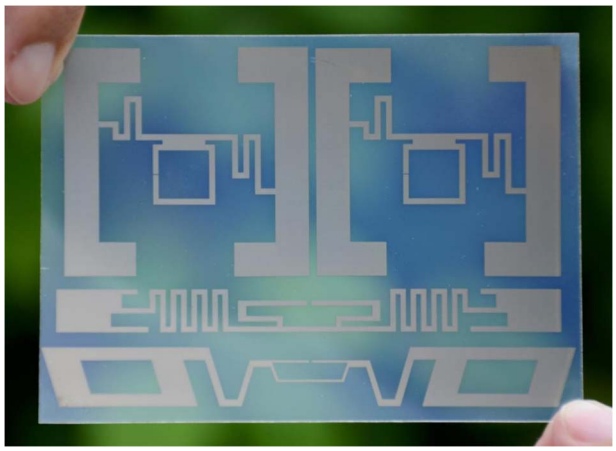

Fig. 6. Ink-jet printed dipole antenna samples using conductive ink with EPSON C88+ printer. From top to bottom: ALN-9634 tag, ALN-9640 tag and UPM Raflatac Short Dipole.

control the flow of the liquid reagent through the nitrocellulose channels.

Target specific antibodies, anti-IgG in this case, are then immobilized on the AuNP Pad where faces the gap of the ink-jet printed antenna. Similar to the operation principle of the lateral-flow immunoassay method [19], the target analyte, IgG in this case, first conjugates with the gold nanoparticle labeled anti-IgG to form a partial sandwich structure (IgG-aIgG-AuNP). When the partial sandwich conjugate is applied to the AuNP Pad, it flows along the nitrocellulose membrane due to its capillary force. Due to antibody-antigen hybridization, a complete sandwich structure, aIgG-IgG-aIgG-AuNP, can be formed when the partial sandwich structured target analytes flow into the area where target specific aIgG is immobilized. The state of the antenna gap region after the formation of sandwich structure is similar to that shown in Fig. 2(a), where the gap is electrically insulated since the gold nanoparticle size is not sufficient large to electrically bridge the split antenna segments. When silver enhancement solution is applied to the SE Pad, it moves through the nitrocellulose channel to the AuNP pad and then adsorption pad through SE apertures. Once the sandwich structure is exposed to the silver enhancement solution, silver ions reduction process occurs. As time progresses, more and more silver ions get reduced on the surface of the gold nanoparticles, as a result of which the size of the shell grows and ultimately electrically bridges the antenna gap [similar to the state that shown in Fig. 2(c)]. The assembly of silver micro-monopole antennas in between the antenna gap tunes the effective length of the ink-jet printed antenna.

III. Materials and Methods

A. Materials

Silver Enhancement Kit, anti-rabbit IgG conjugated with gold nanoparticles, anti-rabbit IgG, IgG, Glutaraldehyde and Methanol were were all purchased from Sigma-Aldrich (St. Louis, MO, USA). Nitrocellulose (NC) membranes with flow rate of 135 sec/4 cm and 180 sec/4 cm were purchased from

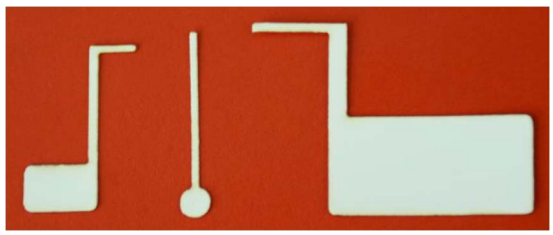

Fig. 7. Nitrocellulose membrane pads cut using a full spectrum laser MLE-40 system. From left to right: SE Pad, AuNP Pad and Adsorption Pad.

Millipore (Billerica, MA, USA). Deionized (DI) water used in the experiment was obtained through Millipore water purification systems (Billerica, MA, USA). The chipset attached to the ink-jet printed antenna was removed from EPC Gen 2 ALN-9640 tag which was purchased from Alien Technology (San Jose, CA, USA). MLE-40 laser system from Full Spectrum Laser (Las Vegas, NV, USA) was used for nitrocellulose membrane pads cutting. An EPSON stylus C88+ ink-jet printer was used to print the antenna structure. The printing substrate and the JS-B25P silver ink were purchased from Novacentrix (Austin, TX, USA). Scanfob Ultra-BB2 Wireless GEN2 UHF RFID Reader/Writer (Cedar Park, TX, USA) was used for remote interrogation and measurements. All the experiments were carried out in a certified Biological Safety Level II laboratory.

B. Procedure

The nitrocellulose membrane was cut into the desired shapes to form SE pad, AuNP pad and Adsorption pad using the MLE-40 laser according to the shapes shown in Fig. 7. Finite-element simulation was used to optimize dipole antenna structure layout to match the impedance of the antenna and the ALN-9640 RFID tag chip. Details of the antenna optimization is provided in [20] and is omitted here for the sake of brevity. The antenna with 80 μm gap was ink-jet printed using EPSON C88+ printer and JS-B25P silver conductive ink on the mesoporous substrate. After antennas have been printed they are annealed in the oven at a temperature of 70 °C for 1 hour. This process facilitated the evaporation of solvent contained in the silver conductive ink and it created a uniform conductance across the antenna structure. The ALN-9640 tag chip was removed from the original tag and was attached to the printed printed antenna using tape, as shown in Fig. 8. Using the procedure described in [12], anti-IgG was immobilized on the nitrocellulose surface of AuNP pad where faces the printed antenna gap. Two SE apertures with a dimension of around 1.0 mm $\times$ 1.5 mm were created on two sides of the gap on the mesoporous substrate as shown in Fig. 8. The AuNP pad was then attached to the antenna using the tape. The two SE apertures were created to provide a path for the silver enhancement solution to flow from SE pad that was attached on the back side of the substrate. The SE pad and the adsorption pad were attached to antenna such that their end-points covered the two SE apertures, separately, as shown in Fig. 8(b). The sequential operation of sample processing can be controlled by the adjusting the length of the flow channel and the pore size of the NC membrane. For instance, silver enhancement procedure requires mixing of the initiator

This article has been accepted for inclusion in a future issue of this journal. Content is final as presented, with the exception of pagination.

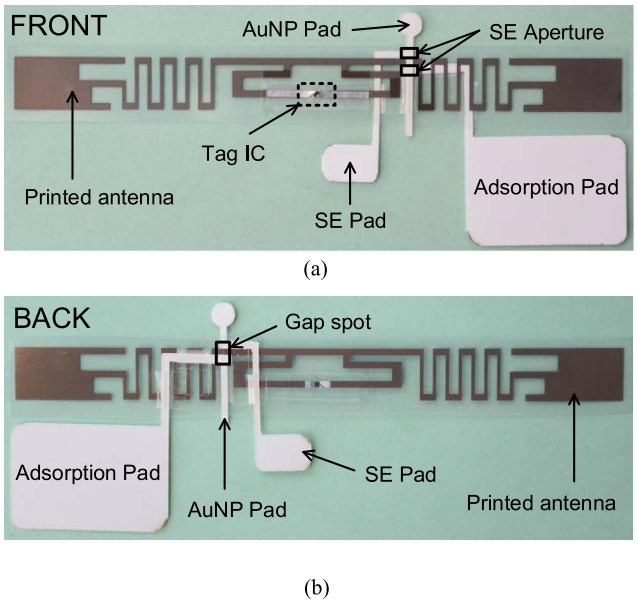

Fig. 8. Photos of the front side and back side of the sensor prototype. (a) Front side of the self-powered microfluidics RFID biosensor prototype. (b) Back side of the self-powered microfluidics RFID biosensor prototype.

and the enhancer solution in a volume ratio of 1 : 1. The silver enhancement solution then flows to the end-point of the SE pad (beneath the SE aperture) which is then drawn by the AuNP pad through SE aperture and then by the adsorption pad if sufficient reagent is provided. During this process, the aIgG-IgG-aIgG-AuNP sandwich structure is exposed to the silver-enhancement solution. Silver ions start to get reduced into metallic silver on the surface of the gold nanoparticles, in the process of which the split segments of the ink-jet printed antenna are being bridged given sufficient time and target analyte. Once this silver micro-monopole antennas' self-assembling process has been finished, the response of the sensor tag was measured using the 915 MHz Scanfob Ultra-BB2 reader. The RFID reader can interface with a laptop through cable or a smartphone through bluetooth for data analysis and display.

IV. Measured Results and Discussions

A. Ink-Jet Printed Gap Using Silver Ink

In this paper, we use ink-jet printing method to print the antenna with gap instead of manually creating the gap on an existing tag [12], [13]. This ensures uniformity of the gap and the procedure can be scaled across many samples. Besides, simulation results in [12] show that a smaller gap length can result in a high sensitivity of the biosensor in the situation when the gap conductance is relatively low. Even though the gap between the electrodes can be bridged by silver micro-monopole antenna chain as shown in Fig. 2(c), the conductance is not as high as that of bulk silver. To improve the sensor's sensitivity, a small gap is therefore preferred. Due to the offset of printer nozzle and the nature that the silver ink is in liquid form, the length of actual printed gap is smaller than that drawn in the layout software. To examine the minimum gap length that can be ink-jet printed, a set of gaps at different sizes (ranging from 60 to 120 μm at a increasing step of 20 μm) are printed using EPSON C88+ printer as shown in Fig. 9(a). Microscope photos of the printed gaps of different lengths are shown in Fig. 9(b)–(e). With the microscope examination of printed gaps, most of the electrodes of the gaps drawn in a length of 60 μm in the layout are electrically shorted as shown in Fig. 9(b).

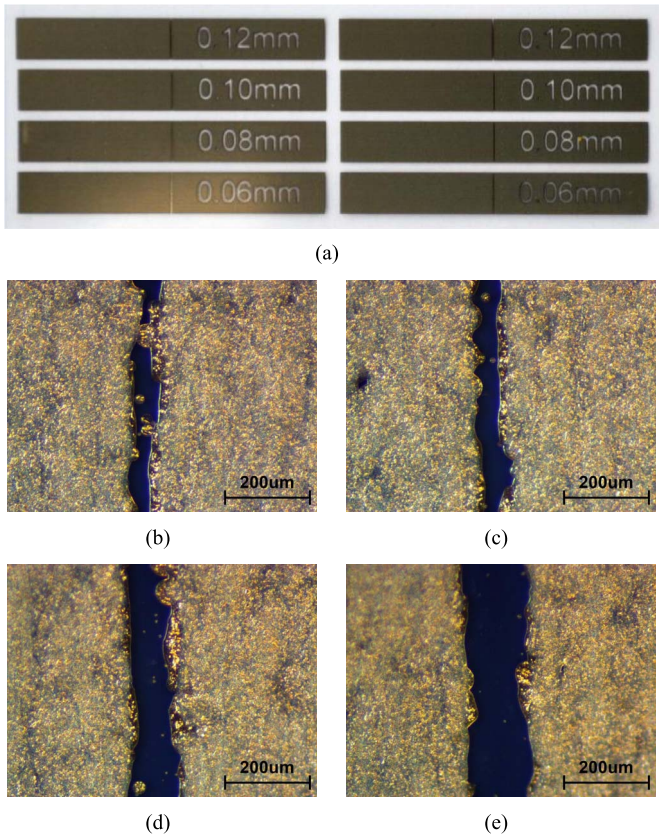

Fig. 9. (a) Photo of silver ink printed gaps with different sizes on the meso-porous substrate using EPSON C88+ printer (sizes of gaps from top to bottom: 120 μm, 100 μm, 80 μm and 60 μm). (b)–(e) Microscope photos of the actual printed gaps at layout sizes of 60 μm, 80 μm, 100 μm and 120 μm, respectively.

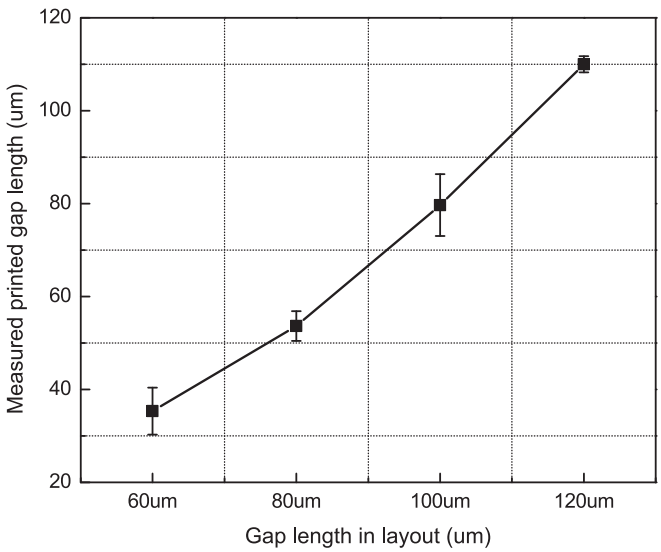

Fig. 10. Comparison of the gap length drawn in layout with the gap length that are printed.

This article has been accepted for inclusion in a future issue of this journal. Content is final as presented, with the exception of pagination.

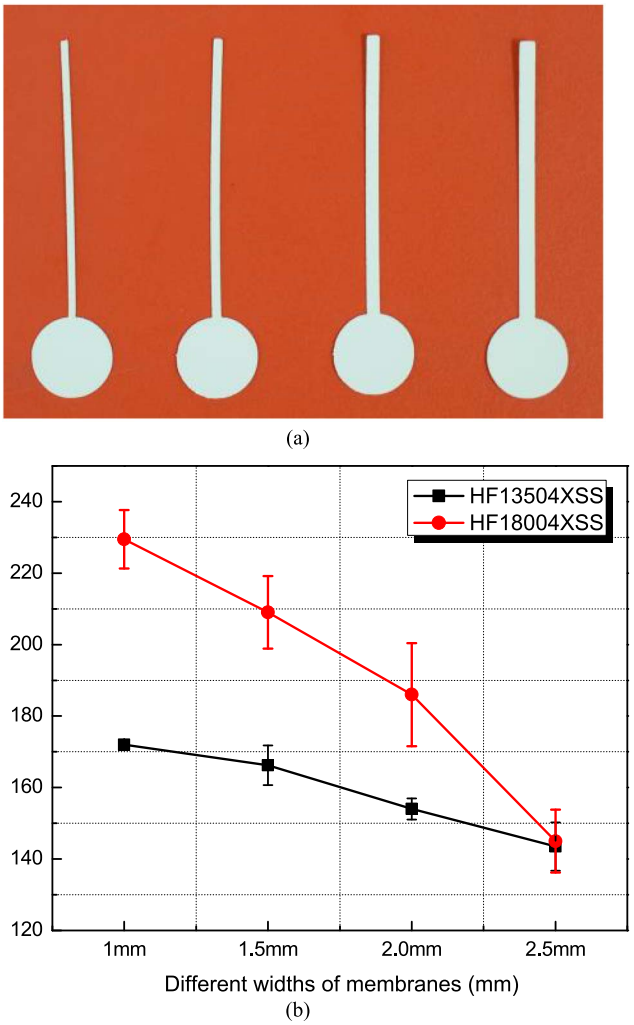

Fig. 11. (a) Nitrocellulose membrane pads of different widths cut using Full Spectrum Laser LLC (MLE-40) for silver enhancement solution flow speed measurement. (b) Flow speed of HF13504XSS and HF18004XSS membrane pads at different widths (1 mm, 1.5 mm, 2.0 mm and 2.5 mm).

A high yield of the printed gaps without ink overlap can be achieved for the gaps drawn at a size equal or larger than 80 μm [Fig. 9(c)–(e)]. A comparison of the lengths of actual printed gaps and the lengths drawn in the layout software is shown in Fig. 10. The lengths of printed gaps are 10 μm to 30 μm smaller than that drawn in the layout. In the implementation of the self-powered micro-fluidics sensor, the antenna with the gap length of 80 μm is ink-jet printed and used.

B. Silver Enhancement Reagent Flow Rate

The liquid flow speed on the nitrocellulose membrane needs to be optimized since it controls how fast the adsorption pad can absorb the silver enhancement solution and how fast the SE pad can transport the liquid. However, accurate measurement of liquid flow-rate in a nitrocellulose membrane is difficult as the rate decays exponentially with respect to the distance [18]. A more common method used to measure the capillary flow is the time needed for the liquid to move and fill completely a membrane of a given length. The pads used for silver enhancement solution flow rate testing are cut into the shapes shown in Fig. 11(a) using MLE-40 laser system. The round reagent application end-point has a dimension of 6 mm in radius. The rectangular liquid flowing areas are 40 mm in length and have different widths ranging from 1 mm to 2.5 mm. During the flow rate measurement 120 μL silver enhancement reagent solution was applied to the reagent application pad using pipette pump. Two different flow rate membranes (HF13504XSS and HF18004XSS) are tested, separately, and the measured silver enhancement reagent flow rate are shown in Fig. 11(b). The detailed parameters and materials of the three pads (SE pad, AuNP pad and adsorption pad) which are used in the implementation of the sensor are listed in the Table I. To note that in the experiment when the silver enhancement solution was applied onto the SE pad with a smaller width, it took a longer time for the reagent to pass through the SE aperture to reach AuNP pad. Our explanation for this phenomena is that if a narrow SE pad is used to guide the silver enhancement reagent to AuNP pad it need more time to aggregate the same amount of the solution at the end-point to pass through the SE aperture and then reach the adsorption pad. This feature can be used to change the monitoring duration by changing the pad width.

TABLE I
MATERIALS AND PARAMETERS OF THREE PADS

	SE Pad	AuNP Pad	Adsorption Pad
Membrane	HF13504XSS	HF18004XSS	HF13504XSS
Width (mm)	2.0	1.5	2.0

C. Measurements Using an Integrated Prototype

The operation of a fully integrated RFID biosensor was verified where the nitrocellulose pads enabled acquisition of the liquid sample acquisition, sample mixing and sample flow to areas where micro-monopole antennas can self-assemble only when target analytes are present. For the fabricated prototypes, the adsorption pad was designed to have a sufficiently large surface area and volume such that it is able to continuously absorb silver enhancement solution diffusing from the SE pad and to facilitate continuous evaporation of the reagent to self-power the diffusion process. Fig. 12 shows a set of photos illustrating a complete process of growing the antenna as the silver-enhancement solution flows through the microfluidic channels. Fig. 12(a) was taken 1 min after the silver enhancement solution was applied through the SE aperture and reached adsorption pad. It can be seen that the silver micro-monopole antennas start to assemble but are not large enough to bridge the antenna gap. The dashed black line on adsorption pad highlights the boundary where the silver enhancement solution filled the pad. It can be seen in Fig. 12(a)–(f) that as time progresses the absorption pad fills up. After 25 minutes, the gap is fully bridged with AuNP cored silver shelled micro-monopole antennas and the split segments of the printed dipole antenna are now electrically bridged. It can be also be seen in Fig. 12(f) that even when the split antenna segments are bridged, the silver enhancement reagent has not filled up the volume of the adsorption pad, which indicates the adsorption pad is still capable to absorb more of the incoming reagent.

This article has been accepted for inclusion in a future issue of this journal. Content is final as presented, with the exception of pagination.

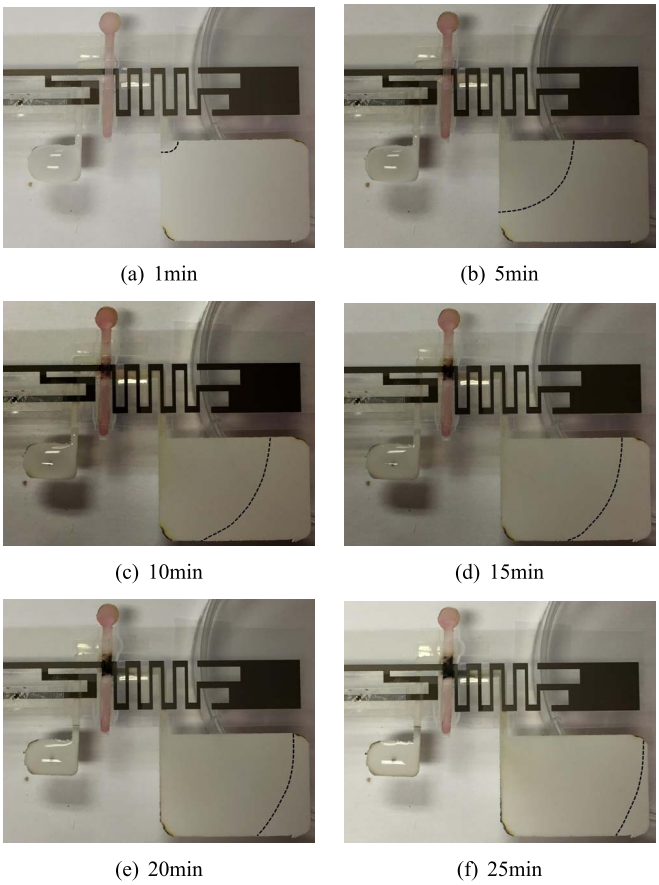

Fig. 12. Demonstration showing that the adsorption pad can continuously absorb the silver enhancement solution during the micro-monopole antenna growth. (a) to (f) show the area covered by absorbing silver enhancement solution after 1 min, 5 min, 10 min, 15 min, 20 min and 25 min separately after the solution path has been formed. The dark dashed lines show the boundaries between the area where silver enhancement reagent front has occupied and where it has not.

D. Experiments Using 915 MHz RFID Reader

The process of bridging the antenna (leading to change in the effective length of the dipole) can be detected wirelessly using an COTS RFID reader. For calibration purposes an unmodified 915 MHz dipole antenna (identical structure as the biosensor dipole but without gap) was also integrated with the biosensor. All interrogation measurements from the biosensors (L_1) were normalized with respect to the measurement obtained from the calibration dipole (L_2). To minimize the mutual loading the sensor tag and the calibration tag were placed next to each other and a ratiometric readout technique was used [12].

The preliminary results that compare the normalized detection range under two situations (shown in Fig. 13): silver enhancement does not occur when the target analyte is absent; silver enhancement process grows the antenna, which bridges the split ink-jet printed dipole antenna. In the first case, the measured farthest interrogation distance is only 23.5% with respect to that of the calibration tag. For the second case that with silver enhancement, the measured maximum interrogation distance increases to 64.6% with respect to that of the calibration antenna. It validates the proof-of-concept of integration of paper based microfluidics in self-powered self-assembled RFID biosensor.

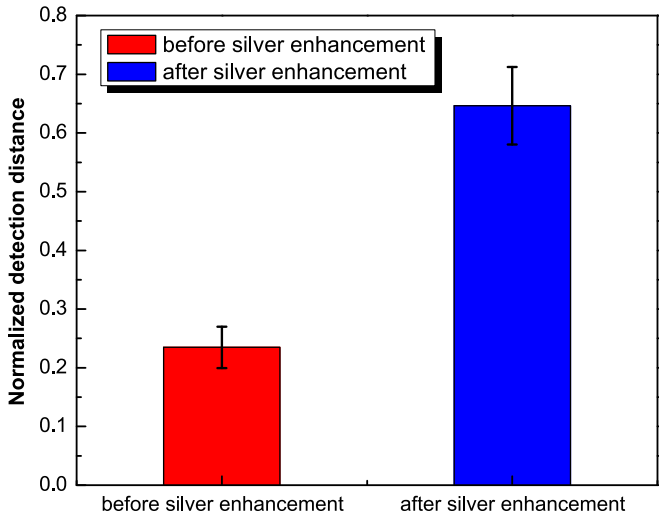

Fig. 13. Measured results validating the proof-of-concept RFID biosensor.

V. Conclusion

In this article we demonstrated the integration of paper-based microfluidics with silver-enhancement based self-assembly for designing a self-powered RFID based biosensing platform. The silver enhancement process self-assembles a micro-monopole antenna and in the process tunes the reflection properties of the RFID tag. Thus, a strong reflected RF signal from the tag signifies the presence of the target analyte. The method of detection presented in this paper can be viewed as a process that transitions from a high-entropy state (detuned and disassembled antenna) to a low-entropy state (tuned and assembled antenna) which is opposite to the effect due to environmental artifacts. Thus, we believe that compared to conventional RFID approaches the proposed method should yield lower false-positives. Verifying this hypothesis using large number of experimental samples will be the objective of future research in this area. In this paper we also demonstrated a low-cost ink-jet printing method that can be used to precisely control the gap length and hence the flow of the silver-enhancement reagent. Nitrocellulose pads were designed, patterned with laser-ablation and integrated on the antenna for sample acquisition, mixing and guiding, serving as reservoirs. The adsorption pad could be designed to be sufficiently large (in volume) to ensure the silver-enhancement solution has enough time to spread and evaporate. Thus the operation of the integrated biosensor is completely self-powered. Future work will focus on enhancing the shelf-life of the biosensing platform and on optimizing the amount of reagent used for analysis. Note that for different types of targets and mediums being analyzed (e.g., milk or blood plasma), the parameters of the microfluidic channels (pore size, gap length and channel length) have to be appropriately optimized. So we envision that while the operational principle of the biosensing platform could remain unchanged, the structure of the platform will be different for each use case.

This article has been accepted for inclusion in a future issue of this journal. Content is final as presented, with the exception of pagination.

REFERENCES

[1] T. San Park, W. Li, K. E. McCracken, and J.-Y. Yoon, "Smartphone quantifies salmonella from paper microfluidics," *Lab on a Chip*, vol. 13, no. 24, pp. 4832–4840, 2013.

[2] J. C. Jokerst, J. A. Adkins, B. Bisha, M. M. Mentele, L. D. Goodridge, and C. S. Henry, "Development of a paper-based analytical device for colorimetric detection of select foodborne pathogens," *Anal. Chem.*, vol. 84, no. 6, pp. 2900–2907, 2012.

[3] J. Noiphung, T. Songjaroen, W. Dungchai, C. S. Henry, O. Chailapakul, and W. Laiwattanapaisal, "Electrochemical detection of glucose from whole blood using paper-based microfluidic devices," *Analytica Chimica Acta*, vol. 788, pp. 39–45, 2013.

[4] J. Yu, L. Ge, J. Huang, S. Wang, and S. Ge, "Microfluidic paper-based chemiluminescence biosensor for simultaneous determination of glucose and uric acid," *Lab on a Chip*, vol. 11, no. 7, pp. 1286–1291, 2011.

[5] Z. Nie, F. Deiss, X. Liu, O. Akbulut, and G. M. Whitesides, "Integration of paper-based microfluidic devices with commercial electrochemical readers," *Lab on a Chip*, vol. 10, no. 22, pp. 3163–3169, 2010.

[6] A. D. Warren, G. A. Kwong, D. K. Wood, K. Y. Lin, and S. N. Bhatia, "Point-of-care diagnostics for noncommunicable diseases using synthetic urinary biomarkers and paper microfluidics," *Proc. Nat. Acad. Sci.*, vol. 111, no. 10, pp. 3671–3676, 2014.

[7] X. Li, D. R. Ballerini, and W. Shen, "A perspective on paper-based microfluidics: Current status and future trends," *Biomicrofluidics*, vol. 6, no. 1, 2012, Art. no. 011301.

[8] V. Mani, K. Kadimisetty, S. Malla, A. A. Joshi, and J. F. Rusling, "Paper-based electrochemiluminescent screening for genotoxic activity in the environment," *Environ. Sci. Technol.*, vol. 47, no. 4, pp. 1937–1944, 2013.

[9] X. Zhu, S. K. Mukhopadhyay, and H. Kurata, "A review of RFID technology and its managerial applications in different industries," *J. Eng. Technol. Manage.*, vol. 29, no. 1, pp. 152–167, 2012.

[10] C. Huang and S. Chakrabartty, "An asynchronous analog self-powered CMOS sensor-data-logger with a 13.56 MHz RF programming interface," *IEEE J. Solid-State Circuits*, vol. 47, no. 2, pp. 476–489, 2012.

[11] M. Yuan, E. Alocilja, and S. Chakrabartty, "A novel biosensor based on silver-enhanced self-assembled radio-frequency antennas," *IEEE Sensors J.*, vol. 14, no. 4, pp. 941–942, Apr. 2014.

[12] M. Yuan, P. Chahal, E. Alocilja, and S. Chakrabartty, "Wireless biosensing using silver-enhancement based self-assembled antennas in passive Radio Frequency Identification (RFID) tags," *IEEE Sensors J.*, vol. 15, no. 8, pp. 4442–4450, Aug. 2015.

[13] M. Yuan, P. Chahal, E. C. Alocilja, and S. Chakrabartty, "Sensing by growing antennas: A novel approach for designing passive RFID based biosensors," in *Proc. IEEE Int. Symp. Circuits and Systems*, May 2015, pp. 2121–2124.

[14] M. Yuan, E. Alocilja, and S. Chakrabartty, "Self-powered wireless biosensing based on integration of paper-based microfluidics with self-assembling RFID antennas," in *Proc. IEEE Biomedical Circuits and Systems Conf.*, Oct. 2015, pp. 1–4.

[15] Y. Liu, D. Zhang, E. C. Alocilja, and S. Chakrabartty, "Biomolecules detection using a silver-enhanced gold nanoparticle-based biochip," *Nanoscale Res. Lett.*, vol. 5, no. 3, pp. 533–538, 2010.

[16] N. K. Thom, K. Yeung, M. B. Pillion, and S. T. Phillips, "Fluidic batteries as low-cost sources of power in paper-based microfluidic devices," *Lab on a Chip*, vol. 12, no. 10, pp. 1768–1770, 2012.

[17] X. Li, J. Tian, and W. Shen, "Progress in patterned paper sizing for fabrication of paper-based microfluidic sensors," *Cellulose*, vol. 17, no. 3, pp. 649–659, 2010.

[18] Rapid Lateral Flow Test Strips: Considerations for Product Development. [Online]. Available: https://www.emdmillipore.com/US/en/products/ivd-oem-materials-reagents/lateral-flow-membranes/n6mb.qB.L0YAAAE_gut3.Lxi,nav

[19] T. C. Tisone and B. O'Farrell, *Manufacturing the Next Generation of Highly Sensitive and Reproducible Lateral Flow Immunoassay*. New York, NY, USA: Springer, 2009.

[20] G. Marrocco, "The art of uhf rfid antenna design: Impedance-matching and size-reduction techniques," *IEEE Antennas Propag. Mag.*, vol. 50, no. 1, pp. 66–79, 2008.

Mingquan Yuan (S'14) received the B.S. degree in electronic science and technology from the Huazhong University of Science and Technology, Wuhan, China, and the M.S. degree in electronics engineering and computer science from Peking University, Beijing, China, in 2009 and 2012, respectively.

From 2012–2015, he was a Research Assistant at Michigan State University, East Lansing, MI, USA. Currently, he is working toward the Ph.D. degree at Washington University in St. Louis, St. Louis, MO, USA. His research interests include passive RFID biosensors, wireless detection, flexible electronics, and micro/nano fabrication.

Evangelyn C. Alocilja (M'87) received the B.S. degree (cum laude) in chemistry from Silliman University, Dumaguete City, Philippines, in 1973, the M.S. degree in soil chemistry/plant physiology from the University of Philippines, Quezon City, Philippines, in 1981, and the M.S. and Ph.D. degrees in systems science/electrical engineering from Michigan State University (MSU), East Lansing, MI, USA, in 1983 and 1987, respectively.

Currently, she is a Professor in the Department of Biosystems and Agricultural Engineering and an Adjunct Professor in the Institute of International Health at MSU. From 1987–1990, she was a Postdoctoral Fellow in Agricultural Engineering, Crop Science, and Electrical Engineering at MSU. From 1991–1992, she was a Research Consultant at the International Rice Research Institute, Laguna, Philippines. In 1992, she was a Research Consultant with the Commonwealth Scientific and Industrial Research Organization, Australia. She is a Coinvestigator of the National Center for Food Protection and Defense, Department of Homeland Security Center of Excellence. Her research interests include the development of nanoparticle-based biosensors for homeland security, food and water safety, and health care.

Shantanu Chakrabartty (S'99–M'04–SM'09) received the B.Tech degree from the Indian Institute of Technology, Delhi, India, in 1996, and the M.S and Ph.D degrees in electrical engineering from Johns Hopkins University, Baltimore, MD, USA, in 2002 and 2004, respectively.

Currently, he is a Professor in the Department of Computer Science and Engineering at Washington University in St. Louis, St. Louis, MO, USA. From 2004–2015, he was an Associate Professor in the Department of Electrical and Computer Engineering at Michigan State University (MSU), East Lansing, MI, USA. From 1996–1999, he was with Qualcomm Inc., San Diego, CA, USA, and during 2002 he was a Visiting Researcher at The University of Tokyo, Tokyo, Japan. His work covers different aspects of analog computing, in particular non-volatile circuits, and his research interests include energy harvesting sensors and neuromorphic and hybrid circuits and systems.

Dr. Chakrabartty was a Catalyst Foundation fellow from 1999–2004, and received the National Science Foundation's CAREER award, University Teacher-Scholar Award from MSU, and the 2012 Technology of the Year Award from MSU Technologies. Currently, he serves as associate editor for IEEE TRANSACTIONS OF BIOMEDICAL CIRCUITS AND SYSTEMS and *Advances in Artificial Neural Systems*, and a review editor for *Frontiers of Neuromorphic Engineering*.